Macromolecular Research, Vol. 24, No. 3, pp 209-217 (2016)
DOI 10.1007/s13233-016-4031-7

www.springer.com/13233
pISSN 1598-5032 eISSN 2092-7673

Preparation, Curing, and Properties of Boron-Containing Bisphenol-S Formaldehyde Resin/*o*-Cresol Formaldehyde Epoxy Resin/Nano-SiO_2 Composites

Weihong Wu[1,2], Jingjing Leng[1], Zheng Wang[1], Hongqiang Qu*[,1], and Jungang Gao*[,1]

[1]*College of Chemistry and Environmental Science, Hebei University, Baoding 071002, P. R. China*
[2]*College of Science, Agricultural University of Hebei, Baoding 071001, P. R. China*

Received June 20, 2015; Revised December 22, 2015; Accepted December 25, 2015

Abstract: Boron-containing bisphenol-S formaldehyde resin (BBPSFR) with different amounts of nano-SiO_2 by *in situ* formation was used to cure *o*-cresol formaldehyde epoxy resin (*o*-CFER). The curing kinetics, dynamic mechanical properties, and thermal stability of BBPSFR/*o*-CFER/nano-SiO_2 composites (BCS) were investigated by differential scanning calorimetry (DSC), dynamic mechanical analysis (DMA), thermogravimetry (TG), and thermogravimetry-mass spectrometry (TGMS). Morphology of nano-SiO_2-containing BBPSFR and glass fiber laminates of the BCS were characterized by transmission electron microscopy (TEM) and scanning electron microscopy (SEM). The mechanical properties and electrical properties were also determined. The results showed that nano-SiO_2 accelerated the curing process and decreased the curing temperature; the non-isothermal curing kinetics of the BCS can be described by the two-parameter (m, n) Šesták-Berggren kinetic model, and the average value of m was 0.32 and n was 1.00. The thermal stability was enhanced by the addition of nano-SiO_2, especially at higher temperatures, and the residual weight increased with increasing nano-SiO_2 content. Incorporation of 6 wt% of nano-SiO_2 increased the impact strength from 105 to 149 kJ/m^2 and storage modulus at ambient from 6.85 to 12.7 GPa, and the TEM photograph of which showed that nano-SiO_2 particles (about 50 nm) were dispersed in the matrix more uniformly. The volume resistance, R_v, and dielectric constant, ε, slightly increased when the nano-SiO_2 content was 3 wt%.

Keywords: epoxy resin, nano-SiO_2, curing kinetics, thermal properties, mechanical properties.

Introduction

Epoxy resin is the most widely exploited generic type of reactive polymeric resin that is widely used in the polymer industry for coatings, structural adhesives, insulating materials, polymeric composite material, *etc*.[1-3] However, the application of epoxy resin is limited in many high-performance application fields because of its low toughness and the thermal deformation temperature of the curing materials. The properties of epoxy resin are directly affected by the structure and properties of the curing agent. All commercial curing agents of epoxy resins can be divided into three basic categories: amine type (especially aromatic and aliphatic amines), anhydride type, and polymer type (polyamide and phenolic resin, *etc.*).[1,4] Amine-type curing agents have a lower curing temperature than anhydride types, but the amine-cured materials have low thermal degradation properties.[5,6] Anhydride-type curing agents need higher curing temperatures and the cured materials have greater brittleness than those cured with other types of curing agents.[7,8] The materials cured by polymer have good physical and mechanical properties, which usually combine the properties of the epoxy resin and the polymeric reagent type.[8-10]

Phenolic formaldehyde resin (PFR) can be used as a curing agent for epoxy. Epoxy resin cured by PFR has a high glass transition temperature, T_g, superior mechanical properties, and thermal resistance.[8] However, the commonly phenolic formaldehyde resin is almost entirely oxidatively degraded at 600 °C.[11] There are two ways to further increase the thermal stability and high-temperature residual weight of PFR, one way is to form boron-containing phenolic (BPFR) resin by introducing the element boron into the molecular chain of the resol and novolac phenolic resins,[12-14] and the other way is to introduce sulfonyl groups, -SO_2-, into the backbone of the polymer. So boron-containing bisphenol-S formaldehyde resins (BBPSFR) were synthesized. BBPSFR had a mechanical loss (tanδ) α peak at 264.4 °C, which is 104 °C higher than that of pure bisphenol-S formaldehyde resins, and 110 °C higher than that of common BPFR.[15]

Epoxy resin-based bisphenol A has been the most extensively applied epoxy resin. However, in the past few years, bisphenol A has been found to have a physiological effect on humans.[16,17] The *o*-cresol formaldehyde epoxy resin (*o*-CFER) is considered to be worthy of further study because it has good

*Corresponding Authors. E-mails: gaojg@hbu.edu.cn or hqqu@163.com

chemical resistance and good electrical and mechanical properties.[18] Also, *o*-cresol does not have a physiological effect on humans, which facilitate its use.

Organic-inorganic hybrid nanocomposite materials have been regarded as a new generation of high-performance materials since they combine the advantages of both inorganic materials and organic polymers. In order to further improve the heat resistance and mechanical properties of epoxy and phenolic resin composites, Conradi *et al.* reported the reinforcement effect of adding silica nanoparticles to the epoxy and phenolic resin.[19-23]

In this work, we have introduced nano-SiO_2 by *in situ* hydrolysis from the hydrolysis of tetraethoxysilane to form nanocomposites of BBPSFR/*o*-CFER (BC) and BBPSFR/*o*-CFER/nano-SiO_2 (BCS). Glass fiber-reinforced laminates of BCS as resin matrices were prepared, and the kinetic parameters of the curing process, the dynamic mechanical properties, morphology, thermal stability, mechanical properties, and electric properties were determined.

Experimental

Materials. Bisphenol-S (BPS), polymeric grade, was supplied by Changsheng Chemical Co. Ltd., China. Formalin, *o*-cresol, epichlorohydrin, tetraethoxysilane (TEOS), isopropanol, NaOH, and boric acid are all analytical reagents and were supplied by Tianjin Chemical Reagent Co., China. According to the literature,[21] *o*-CFER was synthesized and its epoxy equivalent value is 268, the approximate form is shown in Scheme I.

Preparation of BBPSFR/nano-SiO_2 Composites. The BBPSFR was synthesized as follow.[15] 50.0 g of bisphenol-S (0.2 mol), 48.65 g (0.6 mol) of formalin (37 wt%), and 0.723 g of NaOH as a catalyst were added to a 250 cm^3 four-necked flask equipped with a stirrer, thermometer, and a condenser. The mixture was then heated to 94 °C. The mixture was stirred and kept at this temperature until it was clear and transparent. It was maintained under these conditions for 1 h, and then the water was removed under vacuum. In the second stage, 6.60 g of boric acid was added to the mixture and refluxed at 100 °C for 1 h. The water was then removed under vacuum to obtain

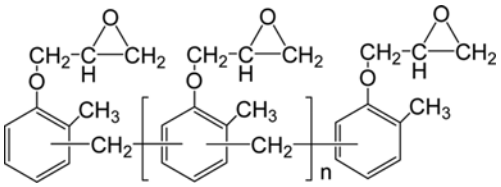

Scheme I. Structure of *o*-CFER.

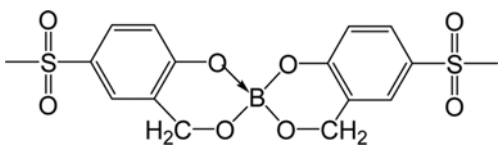

Scheme II. Structure of BBPSFR.

BBPSFR. The BBPSFR/nano-SiO_2 resins were prepared from solutions of BBPSFR in ethanol and stoichiometry parts of water by adding TEOS drop by drop. The mixture was vigorously stirred for 1 h at room temperature, and then refluxed for another 2 h. The water and ethanol were removed under vacuum. The molecular structure of BBPSFR is shown in Scheme II.

Composite Preparation. The glass fiber-reinforced composites were prepared as follows: a pre-treated glass fiber cloth (GF) was immersed in acetone solutions of BBPSFR and *o*-CFER in specific mass ratios of 3:7; the mass ratio of GF and resin was constant at 1:1. After the GF and resin were pre-cured in an oven at 130 °C for approximately 10 min, they were hot pressed at 200 °C and 15 MPa for 30 min to form laminates with dimensions of 25×5×1 mm and 120×120×3 mm. BBPSFR/nano-SiO_2 and *o*-CFER were mixed in a mass ratio of 3:7, and the nano-SiO_2 content in the composites was 0, 3, 6, 9, and 12 wt%. According to the nano-SiO_2 content of the sample, it was labeled as BC, BCS3, BCS6, BCS9, and BCS12, respectively. The laminates with dimensions of 25×5×1 mm and 120×120×3 mm of the BC and BCS were prepared by the same method.

Characterization. The differential scanning calorimeter (DSC, Diamond, Perkin-Elmer Co., USA) was calibrated with high-purity indium and operated under a 20 cm^3/min nitrogen flow rate. Approximately 6 mg of the sample was placed in a sealed aluminum sample pan. Dynamic scans were conducted from 30 to 260 °C at heating rates, β, of 1, 5, 10, 15, 20, and 25 °C/min. The dynamic mechanical behavior of the materials was characterized by a dynamic mechanical analyzer (DMA, Q8000, Perkin-Elmer Co., USA). Glass fiber-reinforced laminates were used to determine the mechanical loss (tanδ) peak temperature, T_p, of the composite. Laminated strips with dimensions of 25×5×1 mm was prepared by hot pressing and curing at 200 °C for 30 min. The samples were heated from 25 to 250 °C at a heating rate of 2 °C/min and a frequency of 2 Hz. Thermogravimetry (TG) of the resin was carried out on a thermogravimetry apparatus (Pyris 6, Perkin-Elmer Co., USA) from 25 to 800 °C in N_2 flow of 20 cm^3/min and 10 °C/min. Thermogravimetry-mass spectrometry instrument (TGMS, STA 449C-QMS 403C, Netzsch Co. Ltd., Germany) was used to analyze degradation fragments of the composite.

According to ASTM D638 and D256, the tensile strength and impact strength were determined at 25 °C and 50% relative humidity. The tensile strength was measured by using an electronic tensile tester (WSM-20KN, Changchun Zhineng Co., China), tests were conducted at an extension rate of 20.0 mm/min. The impact strength was measured by an XCJ-40 impact tester (Chengde Instrument Co., China), and each sample was cut out of a 1.0-mm-deep V-gap. The morphology of the fracture surface of the laminates from the impact test was investigated by scanning electron microscopy (SEM, JSM-7500F, Electro Co., Japan). The fracture surface was plated with a gold film in vacuum and scanned at an accelerating

voltage of 25 kV. Transmission electron microscopy (TEM, JEM-100CX, JEOL, Japan) was used to determine the size and distribution of the nano-SiO_2 particles, the test voltage was 100 kV and the resolution was 0.14 nm. The volume resistivity and surface resistivity of the samples were determined with a ZC36 Megger tester and the test voltage was 250 V. The dielectric constant ε and dielectric loss tangent tanδe of the samples were tested with a QBQ-1B quality factor meter (QBG-3D, Shanghai Electron Equipment Co., China) at a frequency of 2.6 MHz.

Results and Discussion

Influence of Nano-SiO_2 Content on Dynamic Mechanical Properties. Dynamic mechanical analysis was performed to investigate the effect of the nano-SiO_2 on thermal mechanical properties of the nanocomposite. The storage modulus, E', as a function of the temperature of the BCS composites with different amounts of nano-SiO_2 is shown in Figure 1, The storage modulus of BCS3 (12.55 GPa), BCS6 (12.74 GPa) in the glass and rubbery states are dramatically increased by 84% and 86%, respectively, comparing with that of BC at ambient temperature, these increase are attributed to the introduction of nano-SiO_2 into the BBPSFR/*o*-CFER matrix by hydrolysis of TEOS, TEOS undergoes hydrolysis with water and changes into silicic acid, and then converts to nano-SiO_2 by dehydration. The hydroxyl groups on the surface of nano-SiO_2 and the hydroxyl groups of the epoxy matrix can form C-O-C ether link by dehydration and hydrogen bonding or the Van der Waals interaction, which increases the crosslinking degree and rigid of the matrix, so, the storage modulus of BCS is higher than BC.[22,24] However, with the further addition of nano-SiO_2, the increment of storage modulus decrease gradually. The silicic acid will have a tendency to react with each other to form higher average size of nano-SiO_2, which is also reported by Peng,[25] the increasing size of the filler decreases the specific surface, and the storage modulus decreases.[24] The

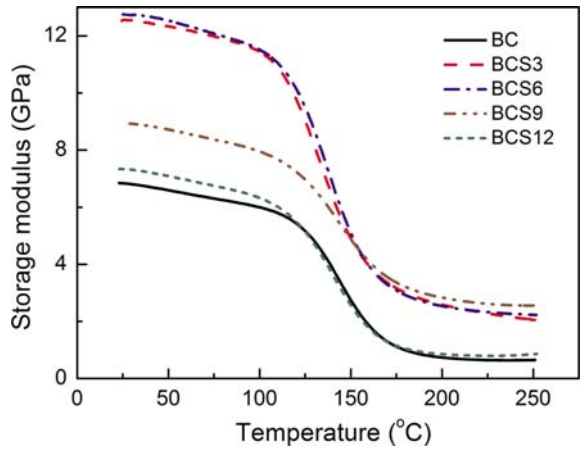

Figure 1. Storage modulus *vs*. temperature curves of GF-BCS composites.

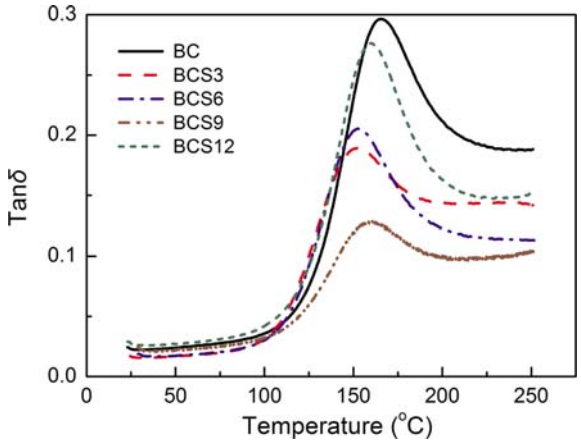

Figure 2. Tanδ *vs*. temperature curves of GF-BCS composites.

rigidity of BCS6 is the highest, which is associated with the fine dispersion of the nano-SiO_2 and the strong interface interaction between it and the matrix.

The values of the transition temperature T_g (1 Hz) taken at the maximum of tanδ versus temperature plots (Figure 2) are used to identify the alpha relaxation associated with the glass transition (T_g). Figure 2 shows that T_g increases with increasing nano-SiO_2 content and the T_g value of BCS3, BCS6, BCS9, and BCS12 is 152.5, 152.9, 159.9, and 160.1 °C, respectively. The enhancing T_g is attributed to increase the crosslink degree by formed C-O-C bonds and the Van der Waals interaction between the surface of nano-SiO_2 and the epoxy matrix,[24] the crosslinking bonds and interfacial interactions can restrict movement of polymeric chain segments to some extent and enhance T_g.[26] However, the T_g of BCS composites is lower than that of BC (163.2 °C). These results are attributed to the fact that the nano-SiO_2 is obtained by hydrolysis of TEOS in ethanol, the presence of residual organics and reduction in the crosslink degree of the polymer matrix.[26] On the other hand, the reaction and Van der Waals interaction between nano-SiO_2 and polymer matrix will decrease the crosslink reaction between polymer molecules, also decrease the crosslink degree of polymer matrix and increase movability of polymeric chain segments. So the BCS has a lower T_g than BC.

Non-Isothermal Curing Kinetics and Activation Energy. Research on the curing reaction kinetics is very important for thermosetting resins because the curing step of thermosetting polymers has a significant influence on the final properties of the material. It is necessary to study the curing kinetics to make it possible to track the extent of a chemical reaction to a given cure system, improve its ultimate application, and develop new materials. Among different techniques employed to study the curing kinetics of these resins, differential scanning calorimetry (DSC) is one of the most commonly used methods. It can provide excellent information about the onset of curing, curing heat, curing completion, and cure reaction conversion, α, so it is important to find a kinetic model that can describe the curing behavior and understand the curing

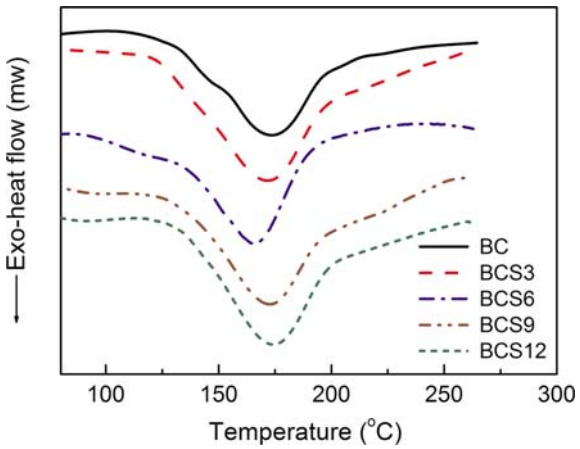

Figure 3. DSC curves of BCS composites.

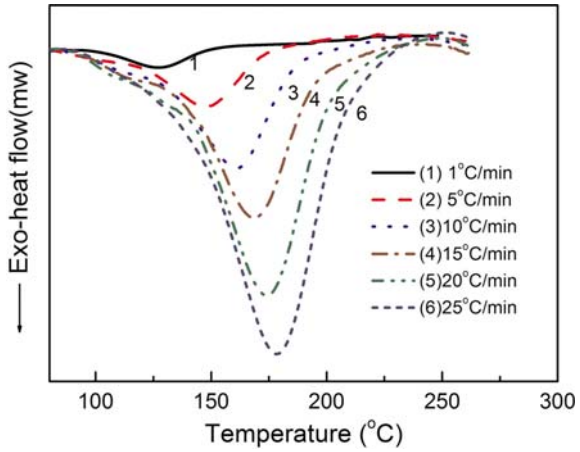

Figure 4. DSC curves of BCS6 at different heating rates.

mechanism.[27,28]

The curing thermograms of the BCS composites are presented in Figure 3. As seen from it, the exothermic peaks are attributed to the curing reaction of this system. BCS6 has a lower initial curing temperature than the other samples. The curing peak temperature of BC is 174.4 ºC, which is higher than that of BCS3 (171.7 ºC), BCS6 (165.8 ºC), BCS9 (172.7 ºC) and BCS12 (174.0 ºC). These results indicate that nano-SiO_2 can accelerate the curing process and decrease the curing temperature. The curing peak temperature initially decreases with increasing nano-SiO_2 content up to 6 wt%; however, at high nano-SiO_2 content, the curing peak temperature increases. The curing temperature of BCS6 is the lowest (165.8 ºC), and it shows that BCS6 has the best distribution of nano-SiO_2 out of all the composites. Thus, the BCS6 can be used to investigate the non-isothermal curing kinetics. Figure 4 shows the typical DSC curves of BCS6 recorded at different heating rates of 1, 5, 10, 15, 20, and 25 ºC/min. As shown in Figure 4, every curve of the sample BCS6 shows an obvious curing peak at approximately 120-179 ºC. The peak temperature shifts to a higher temperature ranges with increasing heating rate, β. Since the movement of the molecular segment is a relaxation motion process, under higher heating rates a higher temperature is required than lower, β, in order to complete the relaxation movement.[29]

In the non-isothermal curing process, an equation based on the isoconversional method can be expressed. Eq. (1) is known as Kissinger's method;[30] it can be applied to different α of the curing process.

$$\ln(\beta/T_\alpha^2) = \ln(AR/E_a) - E_a/RT_\alpha \quad (1)$$

where A is the pre-exponential factor of the Arrhenius equation, T the absolute temperature (K), T_α the temperature of α, R the gas constant (8.314 J/mol/K), β the heating rate, and E_a the apparent activation energy.

For a given α, E_a can be obtained from the plot of $\ln(\beta/T_\alpha^2)$ versus $1/T_\alpha$, and so the E_a values at different conversions can be obtained. According to this method, we can obtain the relationship of E_a and α for these composites. Figure 5 shows the variation of E_a as a function of α. In Figure 5, the linear correlation coefficient r for all values of E_a is between 0.9887 and 0.9963.

As seen from Figure 5, E_a has a slight increase for the pure BC composite. This is because the increasing of crosslinking degree in the curing process decreases the mobility of the unreacted groups, and E_a has a little increase with increasing conversion. But for BCS composites, E_a exhibits only slight variation and remains basically constant for α between 0.05 and 0.80, and then it slowly decreases. This is because the system operates by gelling and diffusion rather than by chemical kinetics at the last stage.[31] BCS composites has a lower E_a than BC composite, as mentioned before, it is because in the BCS composites, there are strong hydrogen bonding and the Van der Waals interaction between the surface of nano-SiO_2 and the epoxy matrix,[24] which accelerates the curing crosslink reaction between resin molecules, and decrease curing reaction E_a until that nano-SiO_2 content is 6 wt%. But, when the TEOS content is higher, the silicic acid will tend to react with each other to form higher average size of nano-SiO_2 rather than to form hydrogen bonds with

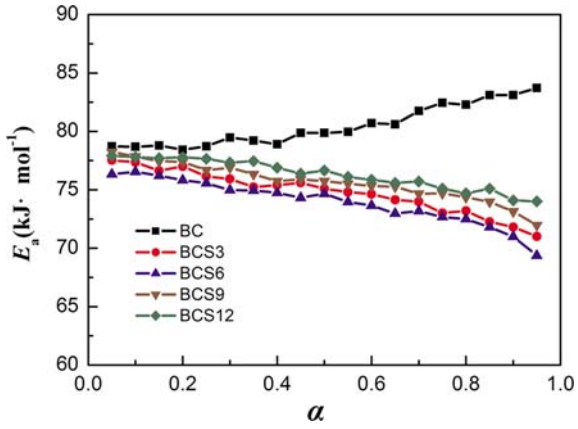

Figure 5. E_a as a function of conversion for BCS composites.

the matrix, which is also reported by Peng,[25] so the acceleration is limited or decreased. The BCS6 has the lowest E_a during the curing process, it is related to the content and the size of nano-SiO_2.

As showed in Figure 5, for BCS6 the difference between the maximum E_a (76.32 kJ/mol) and minimum E_a (69.37 kJ/mol) is small.

The basic assumption for the application of the DSC technique to the curing reaction of the thermosets is the reaction rate, ($d\alpha/dt$), which can be described as follows:[32]

$$\frac{d\alpha}{dt} = k(T)\cdot f(\alpha) \tag{2}$$

where $f(\alpha)$ is a kinetic model function dependent on α and $k(T)$ is a temperature-dependent reaction rate constant that follows an Arrhenius form:

$$k(T) = A\cdot\exp\left(\frac{-E_a}{RT}\right) \tag{3}$$

E_a can be determined by an isoconversional method if the value of $f(\alpha)$ is assumed to be the same for different values of β when α is kept constant. Then the values of E_a can be used to find the appropriate kinetic model which best describes the conversion function of the curing process. The most suitable kinetic model can be evaluated with the functions $y(\alpha)$ and $z(\alpha)$ according to the Eqs. (4) and (5) as follows:

$$y(\alpha) = \frac{d\alpha}{dt}\cdot\exp(x) \tag{4}$$

$$y(\alpha) = \pi(x)\cdot\exp\left(\frac{d\alpha}{dt}\right)\cdot\frac{T}{\beta} \tag{5}$$

where x is the reduced activation energy ($x=E_a/RT$), and $\pi(x)$ is the integral expression of the temperature, which can be well approximated using a fourth rational expression, as in Eq. (6).

$$\pi(x) = \frac{x^3+18x^2+88x+96}{x^4+20x^3+120x^2+240x+120} \tag{6}$$

The $y(\alpha)$ function is proportional to the $f(\alpha)$ function, being

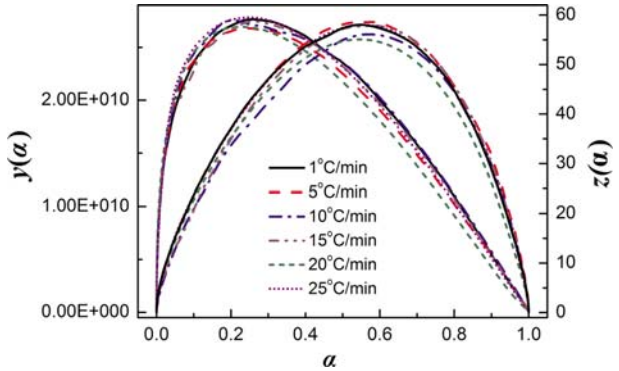

Figure 6. $y(\alpha)$-α and $z(\alpha)$-α curves of sample BCS6 at different heating rates.

Table I. Values of α_p, α_M, and α_p^∞ Obtained from DSC Analysis of BCS6

Heating Rate (°C/min)	α_p	α_M	α_p^∞
1	0.5481	0.2584	0.5058
5	0.5803	0.2458	0.5804
10	0.5720	0.2016	0.5720
15	0.5856	0.2610	0.5856
20	0.5565	0.2474	0.5566
25	0.5529	0.2270	0.5429

characteristic for a given kinetic model. The shape and maximal value of both the $y(\alpha)$ and $z(\alpha)$ function, α_M and α_p^∞, gives valuable information for determining the most suitable kinetic model. Therefore, in this research, the average value of E_a is used to calculate both the $y(\alpha)$ and $z(\alpha)$ functions, using Eqs. (4) and (5), respectively. Figure 6 shows the variation of the $y(\alpha)$ and $z(\alpha)$ functions with α for BCS6 at different heating rates. The values of both $y(\alpha)$ and $z(\alpha)$ are normalized between 0 and 1. From Figure 6, the values of α_M and α_p^∞ [the value of α while $y(\alpha)$ or $z(\alpha)$ are at their maximum value] can be obtained. Table I summarizes all values of α_p, α_M, and α_p^∞ for the BCS6 sample, where α_p is the conversion maximum at the DSC peak. As can be seen from Table I, the α_M values are all lower than the α_p values, $\alpha_M \neq 0$, and $\alpha_p^\infty < 0.632$. In accordance with the kinetic analysis results of Málek under non-isothermal curing reaction conditions, this curing system can also be described by the two-parameter autocatalytic Šesták-Berggren (S-B) kinetic model, shown in Eq. (7).[33]

$$f(\alpha) = \alpha^m(1-\alpha)^n \tag{7}$$

where m and n are the kinetic exponents. According to Eqs. (2) and (3), we then have

$$\frac{d\alpha}{dt} = A\cdot\exp\left(\frac{-E_a}{RT}\right)\cdot\alpha^m\cdot(1-\alpha)^n \tag{8}$$

From Eqs. (2), (3), and (8), we can obtain Eq. (9) as follows:

$$\ln\left[\left(\frac{d\alpha}{dt}\right)e^x\right] = \ln A + n\ln[\alpha^p\cdot(1-\alpha)] \tag{9}$$

where m and n are the reaction orders, $p=m/n$, $x=E_a/RT$, and $p=\alpha_M/(1-\alpha_M)$.

The kinetic parameter n can be obtained from the slope of $\ln[(d\alpha/dt)e^x]$ versus $\ln[\alpha_p(1-\alpha)]$ and the intercept is $\ln A$. The linear correlation coefficients are all between 0.9973 and 0.9962. Table II lists the average values of the E_a, $\ln A$, m, and n as evaluated from the S-B kinetic model for various heating rates, β.

In order to verify the correctness of the S-B kinetic model for this reaction system, the experimentally determined curves of

Table II. Kinetic Parameters of BCS6 from the S-B Autocatalytic Model

Heating Rate β (°C/min)	E_a (kJ/mol)	ln$A$	Mean	p	n	Mean	m	Mean
1	73.96	24.98	24.87	0.35	0.95	1.00	0.33	0.32
5		24.84		0.33	1.00		0.33	
10		24.77		0.26	0.92		0.24	
15		24.88		0.35	1.00		0.35	
20		24.90		0.33	1.04		0.34	
25		24.86		0.29	1.09		0.32	

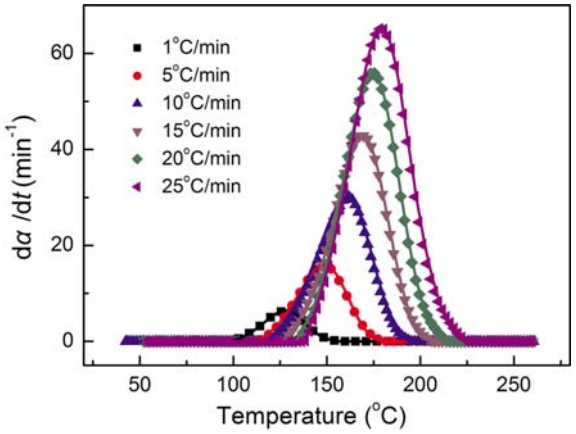

Figure 7. Comparison of experimental data (dots) and simulated values (full lines): plots of reaction rate $d\alpha/dt$ *vs*. temperature for BCS6.

$d\alpha/dt$ versus T (dots) were compared with the simulated curves (full lines) were done. Figure 7 shows the results for sample BCS6. The simulated curves matched the experimental data very well. Thus, we conclude that the two-parameter S-B model can be used for describing the curing kinetics of the system, as seen in Eq. (10).

$$\frac{d\alpha}{dt} = 6.32 \times 10^{10} \exp\left(\frac{-73.96 \times 10^{3}}{RT}\right) \cdot \alpha^{0.32} \cdot (1-\alpha)^{1.00} \quad (10)$$

Thermal Degradation Analysis. Thermal degradation curves are shown in Figure 8, from which it can be seen that when the temperature was lower than 430 °C, the nano-SiO_2 content had little or no effect on the residual weight of the BCS composites. The influence of nano-SiO_2 content on the thermal degradation is mainly seen when the temperature is above 430 °C; in this temperature range, residual weight increases significantly with increasing nano-SiO_2 content. For example, the residual weight percent at 600 °C of samples BC, BCS3, BCS6, BCS9, and BCS12 is 16.39, 30.35, 42.93, 45.83, and 47.71%, respectively. These results demonstrate that the addition of nano-SiO_2 is a good method to improve the thermal stability of the BCS composites, especially when the temperature is higher than 430 °C. The results also demonstrate that the thermal stability of the resin increases with increasing nano-SiO_2 content.

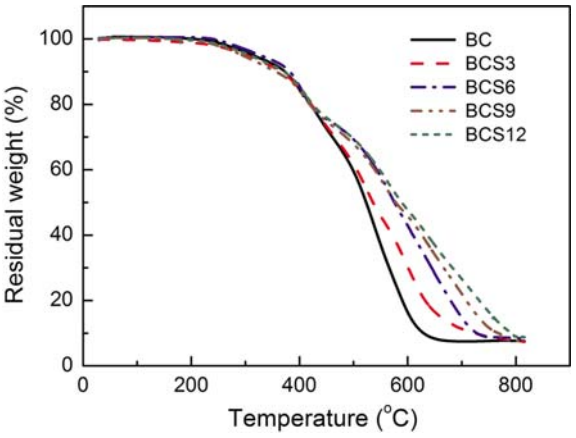

Figure 8. TG curves of BCS composites.

TGMS analysis was utilized to study the volatile species of thermal decomposition and fragmentation processes for BC and BCS6 composites.

It can be observed from Figure 9 that the signals of BC and BCS6 with different ratios of mass-to-charge (m/z) appear within a temperature range of 330-500 °C. Formaldehyde can be determined by the m/z of 30 and acetaldehyde and CO_2 can be determined by the m/z of 44, which come from the decomposition of the epoxy group. MS peaks of SO_2 (with m/z= 64) and its fragment (with m/z=48) come from the decomposition of the bisphenol-S backbone.

From Figure 9(a)-(d), the shapes of the curves for m/z =30, 44, 48, and 64 for BC are similar to those of BCS, and the ion peak intensities of BCS6 are lower than those of BC. These results suggest that the presence of nano-SiO_2 decreases the amount of volatile species resulting from thermal decomposition and that the thermal stability of BCS is higher than that of BC. The ion currents for BC and BCS6, m/z=66, 94 detected in the mass spectrometer are also shown in Figure 9(e), (f), in which m/z=94 is mainly attributed to C_6H_6OH and m/z=66 to a fragment of C_6H_6OH. When m/z is 94, the peak temperature of BCS6 is 433.6 °C, which is 11.4 °C higher than that of BC (422.2 °C). When m/z is 66, the peak temperature of BCS6 is 436.0 °C, which is 21.3 °C higher than that of BC (414.7 °C). The peak temperature of BCS6 increases, which show that nano-SiO_2 inhibits the decomposition of BC and increases its thermal stability.

Mechanical Properties and Morphology. The mechanical

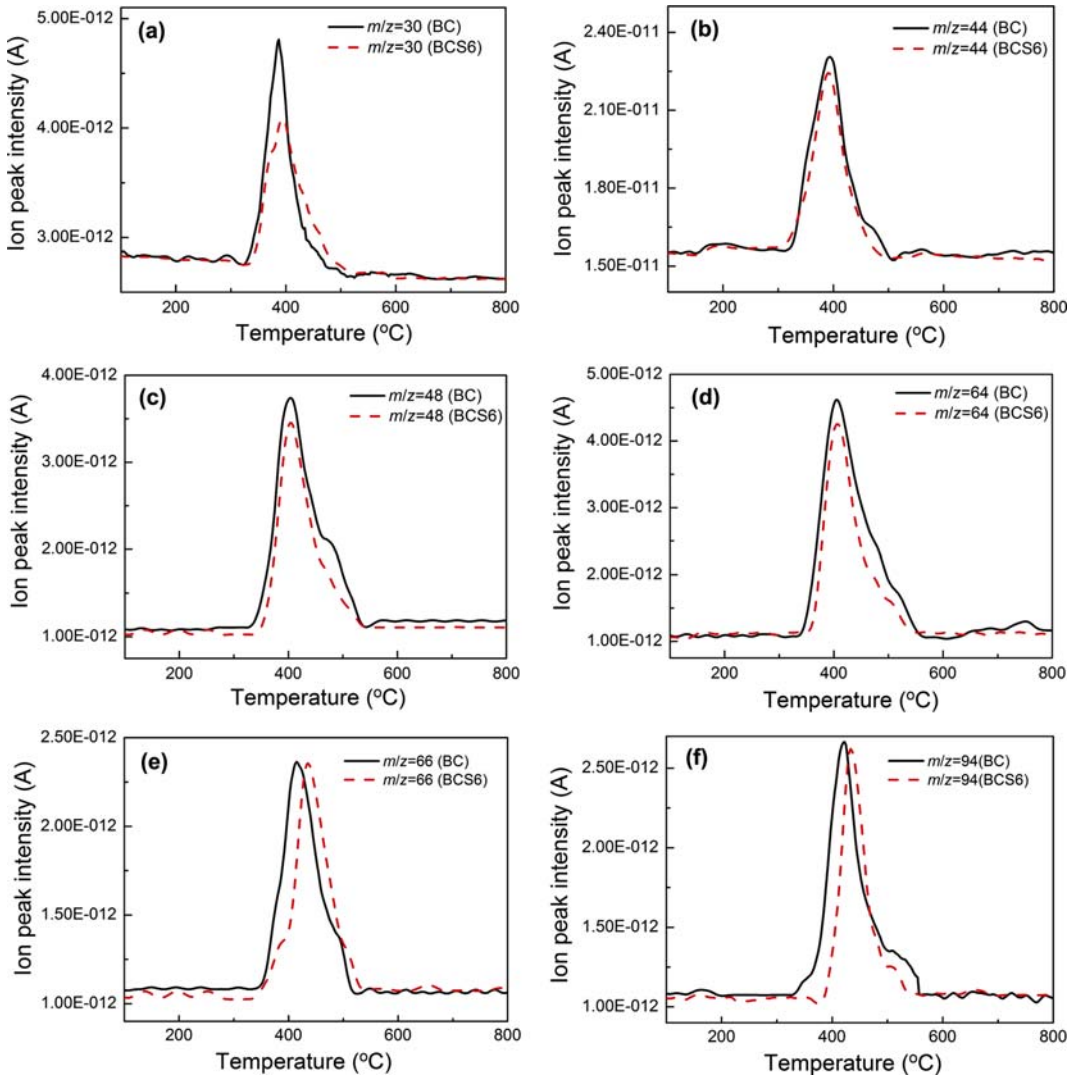

Figure 9. MS profiles of gaseous products of decomposition for BC and BCS6, *m*/*z*=30, 44, 48, 64, 66, and 94.

Table III. Mechanical Properties of BCS Laminates

Sample	Tensile Strength (MPa)	Impact Energy (J)	Impact Strength (kJ/m^2)
BC	156	1.59	105
BCS3	118	2.35	121
BCS6	121	2.57	149
BCS9	111	1.56	84.1
BCS12	93.1	1.52	70.4

properties of glass fiber-reinforced BCS laminates are shown in Table III. As can be seen, the tensile strength of laminates decreases with increasing nano-SiO_2 content. The impact strength is significantly improved when the nano-SiO_2 content is lower. The impact strength of BCS6 is 149 kJ/m^2, which is 44 kJ/m^2 higher than that of BC (105 kJ/m^2). The results are attributed that the nano-SiO_2 particles are uniformly dispersed in matrix, and the inorganic rigid particles presented in BBPSFR/*o*-CFER will induce the formation of microcracks, which will absorb a large amount of the deformation energy and prevent crack growth, thereby enhancing the mechanical properties of the materials.[22,34] However, the higher nano-SiO_2 content reduces the impact strength. When the nano-SiO_2 content exceeds 6 wt%, the impact strength decreases significantly, to less than that of BC, which relates to the congregation of the nano-SiO_2. Figure 10(a) is the TEM photograph of BCS6. As saw from Figure 10(a), the nano-SiO_2 particles are approximately 40-60 nm in diameter and more uniformly dispersed in the matrix. The result of TEM analysis show that *in situ*-formed nano-SiO_2 from TEOS has a more homogeneous distribution in BBPSFR and an organic-inorganic hybrid nanocomposite has been obtained. Figure 10(b) is the SEM photograph of the impact fracture of the BCS6 laminate, and it shows that the conglutination between the resin and glass fibers is good and the dispersion is also good.

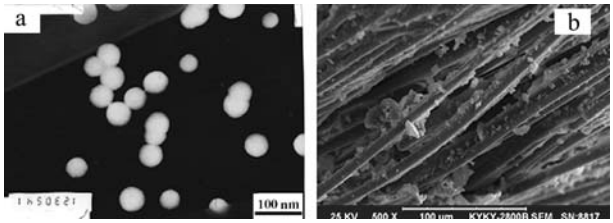

Figure 10. TEM and SEM photographs of BBPSFR/nano-SiO_2 and impact fracture for BCS6 laminate.

Table IV. Electrical Properties of BCS Laminates

Sample	R_v (Ω)	R_s (Ω)	tanδe	ε
BC	4.7×10^{12}	5.8×10^{12}	0.0101	8.221
BCS3	5.3×10^{12}	5.3×10^{12}	0.0124	8.813
BCS6	4.9×10^{12}	5.1×10^{12}	0.0131	8.052
BCS9	3.5×10^{12}	3.5×10^{12}	0.0112	8.057
BCS12	3.8×10^{12}	4.0×10^{12}	0.0112	7.098

Electrical Properties. The electrical properties of glass fiber-reinforced laminates for BCS composites were measured and the results are shown in Table IV. The results show that the volume resistance, R_v, is lower than that of BC laminates when the nano-SiO_2 content exceeds 6 wt%; the surface resistances, R_s, of the BCS laminates decreases with increasing nano-SiO_2 content. The R_v and R_s of BCS are higher than 10^{12} Ω, which indicates that BCS laminates are a good insulating material. The average dielectric loss tangent, tanδe, of BCS laminates is only 0.0120, which is 0.002 higher than that of BC laminate; the dielectric constant, ε, of the BCS laminates is higher than that of BC laminate when the nano-SiO_2 content is only 3 wt%, but it decreases when the nano-SiO_2 content exceeds 6 wt%. One reason for these results is that with increasing nano-SiO_2 content, electrons or ions will gather at the increasing phase interface and enhance the polarization under the action of an external electric field. The other reason is that the formation of cross-linked structure makes it difficult to achieve orientation polarization; as a result, the value of ε decreases.

Conclusions

Boron-containing bisphenol-S formaldehyde resins (BBPSFR) can be utilized to cure *o*-cresol formaldehyde epoxy resin (*o*-CFER). The nano-SiO_2 was adopted in the BBPSFR/*o*-CFER composite by *in situ* polymerization from the hydrolysis of tetraethoxysilane.

The storage modulus and loss modulus are both the highest, when the nano-SiO_2 content is 6 wt%. T_g values of BCS composites are lower than that of BC.

The DSC curves show that nano-SiO_2 accelerates the curing process and decreases the curing temperature. The activation energy values of BCS6 at different conversion calculated by Kissinger's method are similar, and the average value is 73.66 kJ/mol. The non-isothermal curing kinetics of BCS6 can be described by the two-parameter (*m*, *n*) Šesták-Berggren kinetic model, and the average value of *m* is 0.32 and *n* is 1.00.

Thermal stability is enhanced by the addition of nano-SiO_2 especially when the temperature is above 430 °C, the residual weight percent at 600 °C of BCS12 is 47.71%, which is much higher than that of BC (16.39%). The addition of nano-SiO_2 reduces the amount of volatile species resulting from thermal decomposition and inhibits the decomposition of BCS composites, especially at higher temperatures.

The impact strength of BCS6 is 45 kJ/m^2 higher than that of BC (105 kJ/m^2). The volume resistance, R_v, and dielectric constant, ε, slightly increase when the nano-SiO_2 content is 3 wt%; the dielectric loss tangent of BCS6 is the highest.

References

(1) C. A. May. *Epoxy Resins Chemistry and Technology*, Marcel Dekker Inc, New York, 1987.
(2) S. J. Park, G. Y. Heo, F. L. Jin, and K. Y. Rhee, *Macromol. Res*., **23**, 134 (2015).
(3) S. J. Park, G. Y. Heo, and F. L. Jin, *Macromol. Res*., **23**, 320 (2015).
(4) P. A. Mohan, *Polym. Plast. Technol. Eng*., **52**, 107 (2013).
(5) J. T. Wan, Z. Y. Bu, C. J. Xu, B. G. Li, and H. Fan, *Chem. Eng. J*., **171**, 357 (2011).
(6) F. Y. C. Boey and B. H. Yap, *Polym. Test*., **20**, 837 (2001).
(7) M. I. Fan, J. L. Liu, X. Y. Li, J. Cheng, and J. Y. Zhang, *Thermochim. Acta*, **554**, 39 (2013).
(8) W. F. Su, Y. C. Lee, and W. P. Pan, *Thermochim. Acta*, **392-393**, 395 (2002).
(9) S. B. Chen, Q. H. Wang, and T. M. Wang, *J. Reinf. Plast. Compos.*, **32**, 1136 (2013).
(10) U. Konwar, G. Das, and N. Karak, *J. Appl. Polym. Sci*., **121**, 1076 (2011).
(11) J. G. Gao and Y. F. Liu, *Polym. Degrad. Stab*., **63**, 19 (1999).
(12) O. M. Abdalla, A. Ludwick, and T. Mitchell, *Polymer*, **44**, 7353 (2003).
(13) C. Martín, J. C. Ronda, and V. Cádiz, *J. Polym. Sci*., *Part A*: *Polym. Chem.*, **44**, 3503 (2006).
(14) J. G. Gao, H. J. Lin, and W. H. Wu, *J. Macromol. Sci. Part B*: **52**, 512 (2013).
(15) J. G. Gao, W. H. Wu, and X. Li, *Adv. Mater. Res*., **239-242**, 2905 (2011).
(16) H. Okada, T. Tokunaga, X. Liu, S. Takayanagi, A. Matsushima, and Y. Shimohigashi, *Environ. Health Perspect*., **116**, 32 (2008).
(17) F. S. Vom Saal, and C. Hughes, *Environ. Health Perspect*., **113**, 926 (2005).
(18) W. H. Wu, J. G. Gao, Y. Xu, and Q. Y. Xie, *Fiber Polym*., **16**, 664 (2015).
(19) M. Conradi, M. Zorko, A. Kocijan, and I. Verpoest, *Mater. Chem. Phys*., **137**, 910 (2013).
(20) M. G. Veena, N. M. Renukappa, B. Suresha, and K. N. Shivakumar, *Polym. Compos*., **32**, 2038 (2011).
(21) M. Zhao and J. G. Gao, *Thermosetting Resin*, **19**, 20 (2004).
(22) J. Jiao, P. Liu, L. Wang, and Y. Cai, *J. Polym. Res*., **20**, 202 (2013).

(23) K. Kim, J. Nam, S. H. Baeck, K. Lee, S. J. Park, and S. E. Shim, *Macromol. Res.*, **23**, 422 (2015).
(24) J. J. Park, C. H. Lee, J. Y. Lee, and H. D. Kim, *IEEE Trans. Dielectr. Electr. Insul.*, **18**, 667 (2011).
(25) Z. Peng, L. X. Kong, and S. D. Li, *Synth. Met.*, **152**, 25 (2005).
(26) Y. Peng, G. Wang, X. Xue, Y. Takezawa, H. Wang, S. Yamada, Q. Du, and W. Zhong, *Polym. Eng. Sci.*, **48**, 1214 (2008).
(27) R. Hardis, J. L. P. Jessop, F. E. Peters, and M. R. Kessler, *Compos. Part A*, **49**, 100 (2013).
(28) Z. G. Ma and J. G. Gao, *J. Phys. Chem. B*, **110**, 12380 (2006).
(29) A. Atarsia and R. Boukhilir, *Eng. Sci.*, **40**, 607 (2000).
(30) M. A. Vargas, H. Vázquez, and G. Guthausen, *Thermochim. Acta*, **611**, 10 (2015).
(31) S. Vyazovkin, A. Mititelu, and N. Sbirrazzuoli, *Macromol. Rapid Commun.*, **24**, 1060 (2003).
(32) J. Málek, *Thermochim. Acta*, **355**, 239 (2000).
(33) J. H. Hu, J. Y. Shan, J. Q. Zhao, and Z. Tong, *Thermochim. Acta*, **606**, 58 (2015).
(34) H. W. Shi, F. C. Liu, L. H. Yang, and E. H. Han, *Prog. Org. Coat.*, **62**, 359 (2008).